Optical spectroscopy of Yb^{3+} centers in $BaMgF_4$ ferroelectric crystal

J. V. García-Santizo,[1] B. del Rosal,[1] M. O Ramírez,[1] L. E. Bausá,[1,a)] E. G. Víllora,[2] P. Molina,[2] V. Vasyliev,[2] and K. Shimamura[2]
[1]*Dpto. Física de Materiales, Universidad Autónoma de Madrid, 28049 Madrid, Spain*
[2]*National Institute for Materials Science, 1-1 Namiki, Tsukuba 305-0044, Japan*

(Received 11 April 2011; accepted 28 July 2011; published online 16 September 2011)

We report on the optical characterization of Yb^{3+} doped $BaMgF_4$ nonlinear fluoride crystal grown by the Czochralski technique. Low temperature absorption spectroscopy reveals that Yb^{3+} incorporates into the matrix at four well differentiated centers. High resolution site selective experiments have been performed to determine the energy level schemes associated with the major Yb^{3+} centers detected in the system. The fluorescence decay times recorded at 10 K under selective excitation are analyzed for each Yb^{3+} center. The spectroscopic behavior of the codoped Yb^{3+}:Na^{+}:$BaMgF_4$ system has been also investigated. Codoping with Na^{+} eliminates two Yb^{3+} centers present in the singly doped Yb^{3+}:$BaMgF_4$ crystal. The charge compensation mechanisms and site location for Yb^{3+} in the fluoride matrix are discussed. © *2011 American Institute of Physics*. [doi:10.1063/1.3638040]

I. INTRODUCTION

Ferroelectric based photonic devices are nowadays the object of an intense research due to the suitability of their electro-optic and nonlinear properties for light control through a large variety of methods. Light deflectors, optical switchers, multi-frequency converters, or nonlinear optical prisms are some examples of their high potential in photonic applications.[1–4] In the last years, it has been demonstrated that ferroelectric materials can also operate as active optical systems generating laser action when the suitable optically active impurities are incorporated into the crystals. This is for instance the case of $LiNbO_3$, $Sr_xBa_{1-x}Nb_2O_6$ (SBN), and $Ba_2NaNb_5O_{15}$ (BNN).[5–7] The combination of both the nonlinear properties of the ferroelectric crystal host and the light generation by the active ion in a single crystal offers the possibility to obtain multifunctional compact solid state lasers with added functions like self-multifrequency conversion, self-deflection of the coherent radiation, tunability, or even optical bistability.[8]

In this work, we demonstrate the growth of Yb^{3+} doped $BaMgF_4$ (BMF) ferroelectric crystal and we carry out a first spectroscopic characterization of Yb^{3+} ions in this system. BMF is a biaxial orthorhombic crystal with space group C_{2v}^{12} ($Cmc2_1$). At room temperature, it shows a spontaneous polarization of 6.6 $\mu C/cm^2$ with coercive fields exponentially dependent on the applied frequency (from 4 to 24 kV/cm).[9,10] The crystal structure consists of distorted MgF_6 octahedra sharing corners to form puckered sheets parallel to (010). These are linked by Ba^{2+} ions. Both cations, Ba^{2+}, and Mg^{2+} are located in a mirror plane parallel to the (100), in Wyckoff sites 4*a* with a local symmetry C_s.[11] The BMF is an ultra-transparent ferroelectric crystal with a remarkable transparency ranging from the deep UV (126 nm) to the mid-infrared (13 μm).[12] This constitutes an exceptional window for the observation of optical processes or transitions not possible in other systems. Ferroelectric domain engineering has been reported in this material and the first demonstration of second harmonic generation by quasi-phase matching (QPM) with a ferroelectric fluoride has been shown in this system,[13] being the shortest converted wavelength obtained in the UV at 368 nm.[14]

Moreover, doping this fluoride with trivalent rare Earth ions (RE), such as Nd^{3+}, Ce^{3+}, or Pr^{3+}, has already been successfully achieved[15–17] showing the potential of BMF ferroelectric crystals as a nonlinear medium for all solid state lasers in the vacuum-UV/UV mid-infrared wavelength regions.

The incorporation of Yb^{3+} ions is of special relevance due to the good laser properties of this ion for efficient and tunable infrared laser generation under diode pumping.[18,19] In particular, the potential tunability in the near infrared region could be combined with the possibility of QPM in BMF (by multiple gratings or fan-out domain patterning) to generate compact laser sources with a certain range of tunability by self-frequency doubling of the fundamental beam. In this sense, the analysis of the basic spectroscopic properties of Yb^{3+} ions in BMF is a first requirement.

The paper is structured as follows. First, we show the low temperature (LT) (10 K) absorption and luminescence spectra of the Yb^{3+} doped BMF crystal. High resolution site selective measurements are used to determine the crystal field-energy level splitting of the major Yb^{3+} centers detected in the system. The spectroscopy of the codoped Yb^{3+}:Na^{+}:BMF crystal is also analyzed and compared to that of singly doped Yb^{3+}:BMF. Na^{+} atoms are expected to provide the charge compensation mechanism needed when the trivalent Yb^{3+} ions substitute for divalent cations in the crystal lattice. By this means, the charge compensating defects in the Yb^{3+}:BMF crystal decrease and, consequently, a reduction in the multicenter structure is assessed. Finally, the fluorescence decay times recorded at 10 K under selective excitation are analyzed for each center.

a)Author to whom correspondence should be addressed. Electronic mail: luisa.bausa@uam.es.

II. EXPERIMENTAL DETAILS

Yb^{3+} and Yb^{3+}-Na^{+}-doped BMF single crystals have been grown by the Czochralski technique using a 30 kW R.F.-generator. High purity powders (99.99%) of commercially available BaF_2, MgF_2, and YbF_3 were weighed and mixed in a Pt crucible. The Yb^{3+}:BMF crystal was grown from a nominal melt composition of 1 mol. % Yb ($Ba_{1-(x/2)}Mg_{1-(x/2)}Yb_xF_{4+x}$, $x = 0.01$). In order to compensate for the extra valence of Yb^{3+}, the Yb^{3+}-Na^{+} codoped BMF crystal was grown with an additional 1 mol. % of Na^{+} in the form of NaF ($Ba_{1-y}Mg_{1-y}Yb_yNa_yF_4$, $y = 0.01$). Both crystals were grown under CF_4 (99.99%) gas, which was flowed into the furnace before melting the powders at a temperature close to the melting point of BMF, 920 °C. The Yb^{3+} concentration in the grown crystal has been determined by induced coupled plasma mass spectroscopy (ICP-MS) using a ICP-MS Elan 6000 Perkin-Elmer Sciex. The measured value was 0.005 wt. % (0.012 at. % relative to Ba^{2+}), indicating that the incorporation of Yb^{3+} into the BMF matrix is about 100 below the nominal concentration in the melt.

The spectroscopic characterization of Yb^{3+} ions has been mainly carried out by means of absorption, excitation, emission, and fluorescence decay time measurements at LT (10 K). The LT absorption spectra were obtained by means of a Perkin-Elmer Lambda 1050 spectrophotometer provided with an InGaAs detector. For luminescence experiments, an Argon pumped continuous wave tunable Ti:Sapphire laser (Spectra Physics 3900), and a tunable pulsed optical parametric oscillator (Spectra Physics Quanta-Ray 730 MOPO) were used as excitation sources. The photoluminescence spectra were detected with a Peltier-cooled InGaAs detector and with a photomultiplier tube. Lifetime measurements were recorded with a Lecroy digital oscilloscope. In all cases, the sample was cooled down to 10 K by means of a closed cycle He-cryostat. Raman spectra were recorded at room temperature by using a Jobin Yvon spectrometer and a CCD camera. In this case, an Argon laser tuned at 488 nm was used as excitation source.

III. RESULTS AND DISCUSSION

Previous studies on different RE luminescent ions have pointed out that they substitute preferentially for Ba^{2+} ions in the BMF crystal.[16,20] Assuming this lattice site for Yb^{3+} ions, the low C_s symmetry of this cationic position will split the $^2F_{7/2}$ and $^2F_{5/2}$ states of Yb^{3+} ions into 4 and 3 Kramer's doublets, respectively. They will be labeled as $^2F_{7/2}$ (n) ($n = 0,1,2,3$) and $^2F_{5/2}$ (n') ($n' = 0',1',2'$).

Figure 1 shows the LT absorption spectrum of Yb^{3+}:BMF crystal in the 966-980 nm spectral range. The selected region corresponds to the $^2F_{7/2}$ (0) → $^2F_{5/2}$ (0′) single electronic transition of Yb^{3+} ions. The remaining optical transitions, $^2F_{7/2}$ (0) → $^2F_{5/2}$ (1′,2′,3), are not detectable. Four well differentiated peaks are resolved, suggesting the presence of at least four non-equivalent centers, i.e., four different local environments for the Yb^{3+} ion, hereafter labeled as Yb_I, Yb_{II}, Yb_{III}, and Yb_{IV}. The energy positions associated with the $^2F_{7/2}$ (0) → $^2F_{5/2}$ (0′) electronic transition for each center are located at 10247 cm^{-1} (Yb_I∼975.9 nm), 10276 cm^{-1} (Yb_{II}∼973.1 nm), 10300 cm^{-1} (Yb_{III}∼970.9 nm), and 10315 cm^{-1} (Yb_{IV}∼969.5 nm), being the contribution of the Yb_I and Yb_{II}, centers clearly dominant in the absorption spectrum.

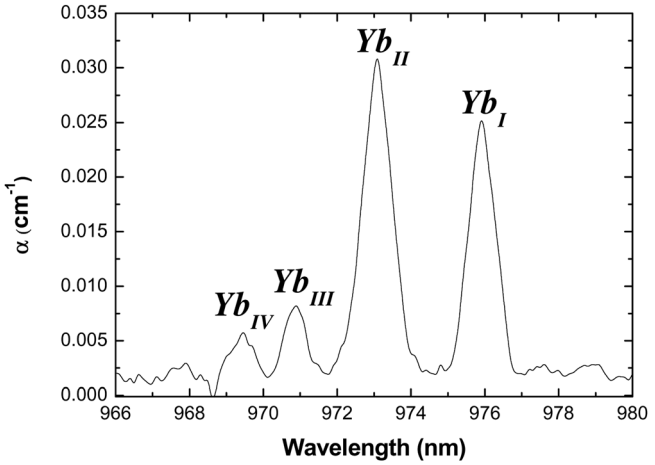

FIG. 1. LT absorption spectrum corresponding to the $^2F_{7/2}(0) \rightarrow {}^2F_{5/2}(0')$ transition of Yb^{3+} ions in $BaMgF_4$.

Figure 2 shows the LT emission spectrum obtained under excitation at 920 nm, at the $^2F_{7/2}$ (0) → $^2F_{5/2}$ (2′) absorption transition. A detail of the spectrum showing the region associated with the $^2F_{5/2}$ (0′) → $^2F_{7/2}$ (0) emission transitions is depicted in the inset. It shows a clear structure that can be well correlated to the multicenter structure observed in the absorption spectrum (Fig. 1). Four emission peaks (marked in the inset) with their maxima at the same positions than those detected in the absorption spectra can be well related to the to the Yb_I, Yb_{II}, Yb_{III}, and Yb_{IV} centers. Additionally, the higher sensitivity and the better spectral resolution of the fluorescence spectroscopy relative to that of the absorption allow to distinguish a doublet structure around the most intense line with two maxima peaking at 972.1 and 973.1 nm. In agreement with previously reported data obtained from other Yb^{3+}-doped fluoride systems,[21] the spectrum in Fig. 2 shows that the contribution of the $^2F_{5/2}$ (0′) → $^2F_{7/2}$ (0) line relative to the other emissions is largely dominant. Additionally, it has

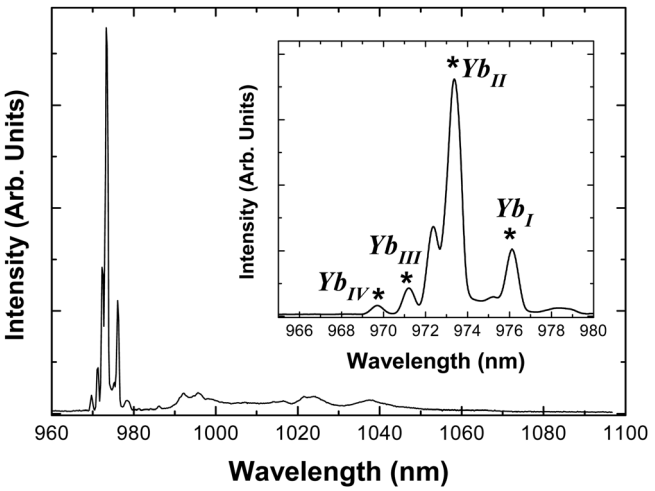

FIG. 2. LT emission spectrum obtained under excitation at 920 nm. The inset shows a detail of the $^2F_{7/2}(0) \rightarrow {}^2F_{5/2}$ (0′) transition to highlight the multisite contribution.

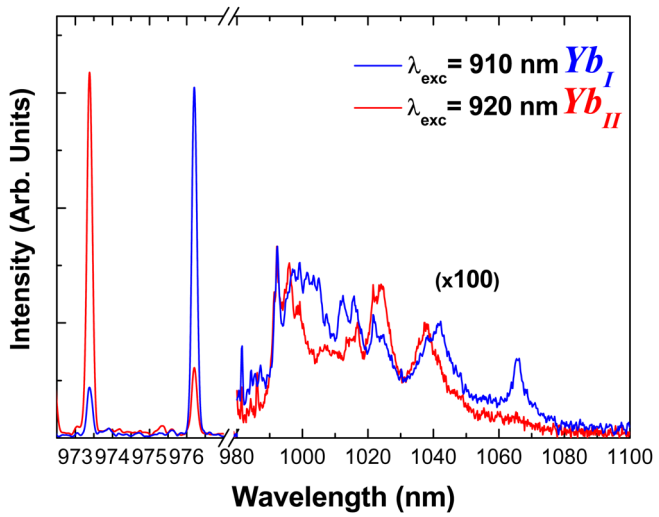

FIG. 3. (Color online) Site-selective emission spectra of Yb^{3+} at LT for the two dominant Yb^{3+} centers (Yb_I and Yb_{II}) in $BaMgF_4$. Excitation wavelengths were, respectively, fixed at 910 and 920 nm for sites Yb_I and Yb_{II}. For the sake of clarity, the region 980-1100 nm has been multiplied by a factor 100.

been confirmed that the low Yb^{3+} concentration prevents reabsorption of the $^2F_{5/2}$ (0′) → $^2F_{7/2}$ (0) emission transition. Since the presence of different centers can play an important role in the optical properties of the Yb^{3+}:BMF system, high resolution site selective spectroscopy is a previous requirement to understand the optical behavior of Yb^{3+} ions in this crystal. Figure 3 shows the LT emission spectra recorded under selective excitation for the Yb_I ($\lambda_{exc} = 910$ nm) and Yb_{II} ($\lambda_{exc} = 920$ nm) centers. The spectra have been normalized to the intensity of the $^2F_{5/2}$ (0′) → $^2F_{7/2}$ (0) emission line. The emission at the 980-1100 nm spectral region has been multiplied by a factor 100 in order to visualize the $^2F_{5/2}$ (0′) → $^2F_{7/2}$ (1,2,3) transitions of Yb^{3+} in BMF. The main difference between those two emission spectra concerns the positions of the $^2F_{5/2}(0') \rightarrow {}^2F_{7/2}(0)$ transitions, which can be well resolved under selective excitation. They are located at 975.9 and 973.1 nm in agreement with those associated with the Yb_I and Yb_{II} centers, respectively. The remaining part of the spectra shows a relatively similar spectral shape for both Yb_I and Yb_{II} centers. The observed broad bands are related to the strongly phonon coupled $^2F_{5/2}(0') \rightarrow {}^2F_{7/2}(1,2,3)$ transitions typical of trivalent ytterbium ion doped crystals.[22] The comparison of these emission spectra shows some differences at around 1010, 1040, and 1065 nm, which allow the assignment of the $^2F_{5/2}(0') \rightarrow {}^2F_{7/2}(1,2,3)$ transitions associated with each center, as will be shown later.

The site selective LT excitation spectra associated with Yb_I and Yb_{II} centers are shown in Fig. 4. The emission wavelength was fixed at their respective $^2F_{5/2}(0') \rightarrow {}^2F_{7/2}(0)$ transitions, at 975.9 nm and 973.1 nm for Yb_I and Yb_{II}. The spectra show the presence of broad bands which can be related to strongly phonon-coupled transitions involving the upper components of the split $^2F_{5/2}$ excited state. In fact, previous studies pointed out the importance of electron-phonon interaction in Yb^{3+} doped crystals.[23] Note that even when the contribution of the $^2F_{7/2}$ (0) → $^2F_{5/2}$ (1′,2′) optical transitions is noticeably weaker than that obtained for the $^2F_{7/2}$ (0) → $^2F_{5/2}$ (0′) transitions, the spectral differences allow the discrimination of the contribution of both centers. For the Yb_I center (Fig. 4(a)), two main optical transitions are observed at 910 nm and 935 nm, while for the Yb_{II} center (Fig. 4(b)) its optical bands are centered at 923 nm and 959 nm. The additional structure observed at lower energy (see, for instance, the peaks at 946 nm for Yb_I and 964 nm for Yb_{II}) can be related to vibronic structure as will be shown.

At this point, it is important to recall that, although the electronic structure of Yb^{3+} ions is simple, the optical spectra related to the transitions among the split sublevels of both $^2F_{7/2}$ fundamental and $^2F_{5/2}$ excited state can be rather complex due to the electron-phonon coupling. The most typical spectral features due to electron-phonon coupling in Yb^{3+}

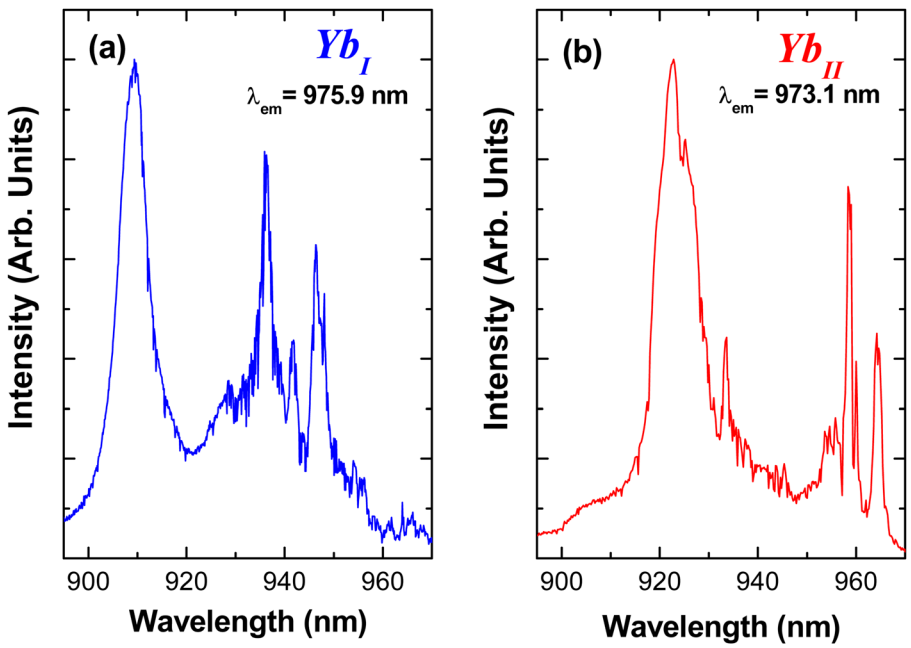

FIG. 4. (Color online) LT excitation spectra associated with the (a) Yb_I site ($\lambda_{em} = 975.9$ nm) and the (b) Yb_{II} center ($\lambda_{em} = 973.1$ nm) in $BaMgF_4$.

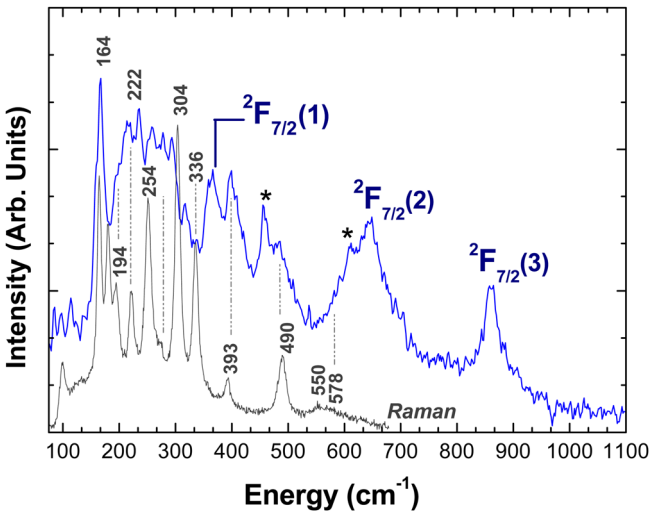

FIG. 5. (Color online) Comparison between the unpolarized Raman spectrum and the LT (10 K) emission spectrum corresponding to the Yb_I center in $BaMgF_4$. The electronic Stark sublevels $^2F_{7/2}$ (1,2,3) and the main Raman modes have been labeled in the figure.

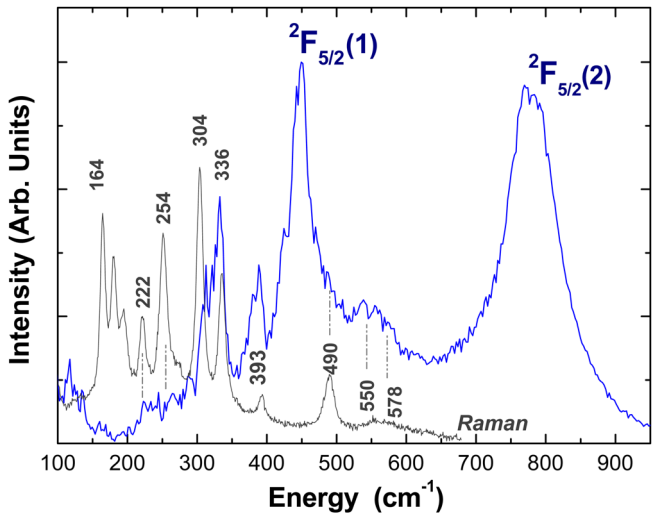

FIG. 6. (Color online) Comparison between the unpolarized Raman spectrum and the LT (10 K) excitation spectrum corresponding to the Yb_I site. The Stark sublevels $^2F_{5/2}$ (1,2) and the main Raman modes are labeled on the figure.

doped optical systems include spectral broadening, asymmetries, splitting, vibronic sidebands, etc., which makes the identification of the pure electronic transitions in the optical spectra difficult. The problem becomes particularly complicated with the presence of Yb^{3+} multicenters. Here, the rich and complicated excitation and emission spectra of Yb^{3+} ions in BMF have been clarified and the origin of most of the peaks has been identified by comparison with the Raman spectrum of BMF. This comparison shows that most of the optical phonons of BMF effectively couple to the $^2F_{7/2}(0) \rightarrow {}^2F_{5/2}(0')$ electronic transitions of the different centers.

Figure 5 shows the room temperature unpolarized Raman spectrum measured on a *c*-cut BMF crystal together with the LT site selective emission spectrum of the Yb_I center. The abscissa for the emission spectrum corresponds to the absolute energy difference between the energy of the $^2F_{5/2}(0') \rightarrow {}^2F_{7/2}(0)$ transition and the emitted photons of the $^2F_{5/2}(0') \rightarrow {}^2F_{7/2}(1,2)$ transitions. The Raman peaks are in good agreement with previous reported data which showed that the Raman active modes lie within the region of 0–600 cm^{-1}.[24] As can be seen, a good part of the structure on the emission spectrum, particularly that in the low energy region, correlates well with the Raman modes of BMF. Indeed, in the 100-400 cm^{-1} spectral range, almost all the spectral features in the emission spectrum can be associated with a Raman mode except for the peak located at 365 cm^{-1}, which is related to the electronic $^2F_{5/2}(0') \rightarrow {}^2F_{7/2}(1)$ transition. The $^2F_{7/2}(2)$ and $^2F_{7/2}(3)$ Stark sublevels of the Yb_I center can be located at 645 cm^{-1} and 857 cm^{-1}, respectively. The contribution of the Yb_{II} center to the site selective emission spectrum of the Yb_I center due to the spectral overlap has been marked with stars in the figure.

The analogous comparison between the Yb_I excitation and the Raman spectra is shown in Fig. 6. In this case, the abscissa for the excitation spectrum corresponds to the energy difference between the $^2F_{7/2}(0) \rightarrow {}^2F_{5/2}(0')$ transition and the absorbed photons of the $^2F_{7/2}(0) \rightarrow {}^2F_{5/2}(1',2')$ transitions. In a similar way to the previous case, most of the optical phonons of BMF effectively couple to the $^2F_{7/2}$ (0) $\rightarrow$ $^2F_{5/2}$ (0′) electronic transition of Yb^{3+} ions. From Fig. 6, the assignment of the positions of the $^2F_{5/2}(1')$ and $^2F_{5/2}(2')$ Stark sublevels can be made. They can be located 450 cm^{-1} and 785 cm^{-1} above the $^2F_{5/2}(0')$ level, respectively. It should be mentioned here that the comparisons of both excitation and emission spectra with the Raman spectra collected along the *a* and *b* directions lead to the same assignments of the electronic Stark sublevels.

A similar analysis was performed to determine the energy position of the Stark sublevels of the $^2F_{7/2}$ and $^2F_{5/2}$ states of the other dominant center, Yb_{II}. The results are shown in Fig. 7, where the energy level schemes of the $^2F_{7/2}$ and $^2F_{5/2}$ states for the two dominant Yb_I and Yb_{II} centers in the BMF crystal are depicted.

Further information on the spectroscopic behavior of the system can be obtained by codoping the system with Na^+ ions, which are expected to introduce charge compensation mechanisms required when Yb^{3+} ions substitute for divalent

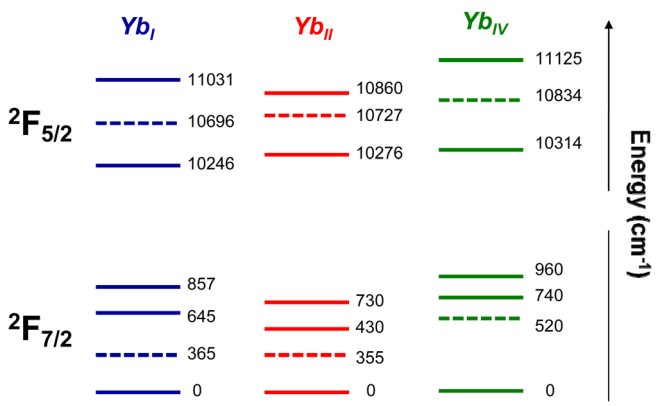

FIG. 7. (Color online) Energy level scheme of the Yb_I, Yb_{II}, and Yb_{IV} centers in $BaMgF_4$.

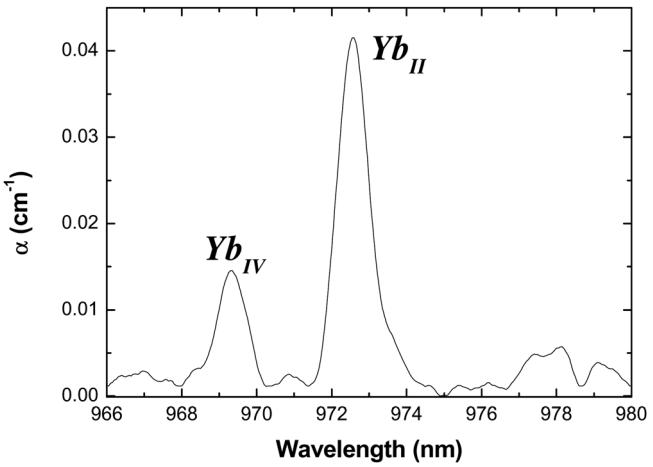

FIG. 8. LT absorption spectrum corresponding to the $^2F_{7/2}(0) \rightarrow {}^2F_{5/2}(0')$ transition of Yb^{3+} ions in the Na^+-Yb^{3+} co-doped $BaMgF_4$.

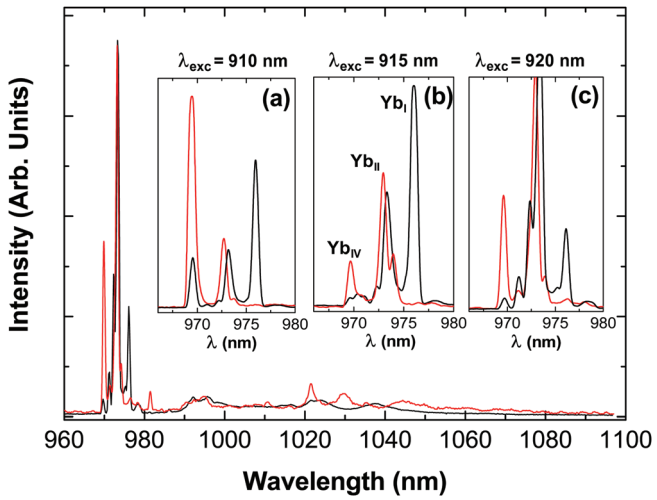

FIG. 9. (Color) LT emission spectra obtained in the Yb^{3+} singly doped (black line) and the Yb^{3+}-Na^+ codoped $BaMgF_4$ (red line). The inset shows a detail of the $^2F_{5/2}$ (0′) → $^2F_{7/2}$ (0) transition for different excitation wavelengths.

cations in the crystal. Figure 8 shows the LT absorption spectrum of Yb^{3+}-Na^+ codoped BMF obtained under the same conditions and in the same spectral range as that of the Yb^{3+} singly doped BMF crystal (Fig. 1). As seen, the distribution of Yb^{3+} centers is strongly modified when Na^+ ions are incorporated into the crystal. In fact, two main features are observed. First, the incorporation of Na^+ in the crystal practically eliminates the contribution of the Yb_I and Yb_{III} centers to the absorption spectrum. Second, an increase in the absorption coefficient of both Yb_{II} and Yb_{IV} centers relative to the case of the singly doped crystal is observed. At this point, it is important to point out that Na^+ ions are not preventing the incorporation of Yb^{3+} ions into the BMF crystal, since the area under the absorption spectrum remains constant after the Na^+ incorporation. A more detailed analysis of Fig. 8 also reveals a larger contribution of the Yb_{IV} center relative to the Yb_{II} one with respect to the case of the singly doped crystal and a very slight blue shift of the $^2F_{7/2}$ (0) → $^2F_{5/2}(0')$ transition of the Yb_{II} center (4 cm^{-1}). All the above mentioned features arise from the incorporation of Na^+ into the BMF host crystal. According to previous reports, Na^+ ions also incorporate into the matrix at the Barium site.[25] As a consequence, not only the charge compensation defects but also the available Ba^{2+} sites for Yb^{3+} ion can be modified and, therefore, its optical response. The lowest limit of the Na^+ content in the codoped crystal has been estimated taking into account the percentage of Yb^{3+} centers which are annihilated after Na codoping (42.5%). The Na^+ concentration must be at least 0.005 at. % relative to Ba^{2+}, which corresponds to the content of the two Yb^{3+} centers (I and III) whose spectral contribution disappears after Na^+ incorporation.

The comparison between the LT emission spectra of Yb^{3+}:BMF and Yb^{3+}:Na^+:BMF is shown in Fig. 9. The spectra were collected in both systems under identical experimental conditions. The differences between both systems are clearly observed on the $^2F_{5/2}$ (0′) → $^2F_{7/2}(0)$ transitions and in turn these are in good agreement with the results observed in the LT absorption spectra of both crystals. The most remarkable feature is related to the emission line associated with the Yb_I center at 976 nm, which disappears completely in the spectra of the Yb^{3+}-Na^+ codoped BMF crystal. The insets show details of the site selective experiments in the $^2F_{5/2}$ (0′) → $^2F_{7/2}(0)$ transition region under excitation at three different wavelengths resonant with the $^2F_{7/2}$ (0) → $^2F_{5/2}(2')$ transitions of the Yb_I, Yb_{II}, and Yb_{IV} centers. As can be seen, as the excitation changes, the relative contribution of the different Yb^{3+} centers varies accordingly. From the comparison between the spectra of both crystals, it can be confirmed that the incorporation of Na^+ into the lattice eliminates the contribution of the Yb_I center. In addition, it produces a clear enhancement of the contribution of the Yb_{IV} center. On the other hand, the presence of Na^+ does not substantially affect the energy position of the two remaining Yb_{II} and Yb_{IV} centers, which would suggest that the charge compensation mechanism for those centers is not local, in a similar way to previous results on Nd^{3+} doped BMF.[15]

Since the Yb_{IV} center becomes one of the two dominant centers in the Yb^{3+}:Na^+:BMF crystal, it is possible to determine its energy level scheme by means of selective excitation and emission. Figure 10(a) and 10(b) show these spectra obtained by monitoring/exciting at the $^2F_{5/2}$ (0′) ↔ $^2F_{7/2}$ (0) optical transitions at 969.5 nm. From the site selective emission spectra, the positions of the $^2F_{7/2}$ (1,2,3) sublevels can be located at 520, 740, and 960 cm^{-1} (1021 nm, 1044, and 1069 nm), respectively, and those of the $^2F_{5/2}$ (1′,2′) state at 10 834 and 11 125 cm^{-1} (923 and 900 nm), respectively, as follows from the excitation spectrum. The lines at 1021 nm (emission) and 923 nm (excitation) could be enhanced by the active Raman mode at around 490 cm^{-1} by coupling to the $^2F_{5/2}$ (0′) ↔ $^2F_{7/2}$ (0) transitions occurring at 969.5 nm.

Taking into account the results of the optical absorption and the site selective spectroscopy, the crystal field energy level diagram corresponding to the Yb_{IV} center in BMF crystals has been obtained. It is shown in Fig. 7, where a comparison with the other dominant centers in the crystal, Yb_I and Yb_{II}, is made. The low signal of the Yb_{III} does not allow its appropriate analysis. The dashed lines in the figure mark

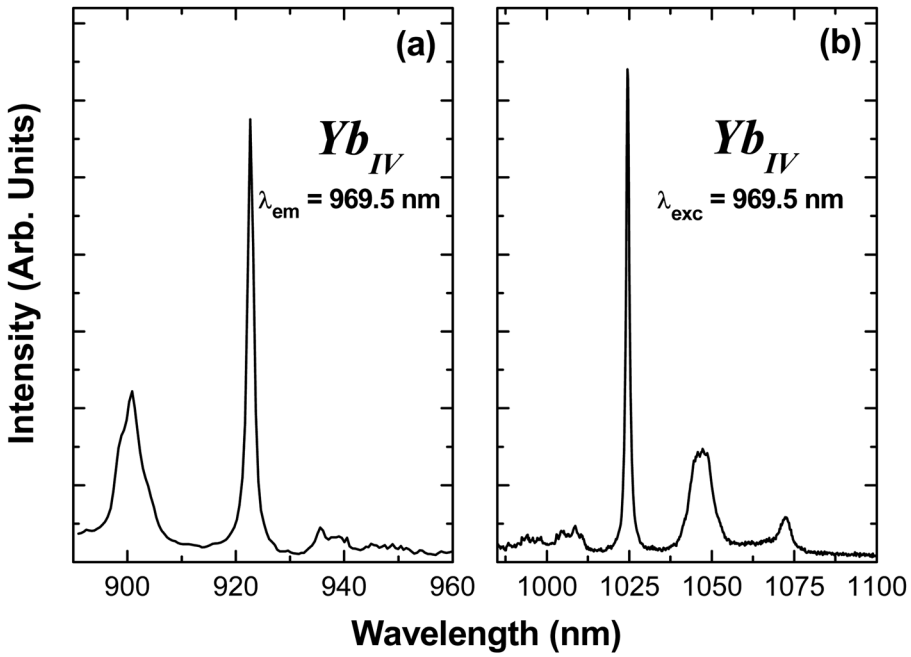

FIG. 10. LT site-selective excitation (a) and emission spectra (b) of the Yb_{IV} center in $BaMgF_4$.

energy positions that cannot be definitively assigned to electronic levels due to the strong mixing with vibration overtones. As observe, the ground state splitting is quite different depending on the center. Differences as large as 230 cm^{-1} are observed and the total splitting of the $^2F_{7/2}$ fundamental state varies from 730 cm^{-1} of Yb_{II} center up to 960 cm^{-1} of Yb_{IV} center. These values are substantially larger than those obtained for other Yb^{3+} doped fluorides, which could be of interest to fulfill the requirements for a potential quasi-four-level laser material.[26]

At this point, the presence of nonequivalent Yb^{3+} centers in the BMF and their main spectroscopic features have been demonstrated. In this respect, it should be taken into account that the incorporation of Yb^{3+} in the $BaMgF_4$ crystal is affected not only by the different size of the ionic radii (the ionic radius of Yb^{3+} is 112 pm, while the ionic radii of Ba^{2+} and Mg^{2+} are 156 and 86 pm, respectively),[27] but also by the valence state of the doping ion. As mentioned, several previous studies have pointed out that luminescent lanthanide ions substitute for Ba^{2+} cations in the BMF crystal lattice. This fact can be justified on the basis of the well-established set of ionic radii published by Shannon,[27] since lanthanide ions are too large to be easily accommodated in the Mg^{2+} octahedral site in the BMF lattice. On the other hand, the presence of non-equivalent centers has also been reported, though the multicenter structure of lanthanide luminescent ions in BMF differs depending on the ion and on the synthesis conditions. For trivalent Ce^{3+} ions, two different Ce^{3+} centers at the Ba^{2+} cationic site have been detected in both, Ce^{3+} singly doped and Ce^{3+} and Na^+ codoped BMF. In this case, the two centers have been related to the presence of a commensurate superstructure of the basic crystal structure of BMF.[15,28] A different origin has been proposed for the center structure in Eu^{2+} doped $BaMgF_4$. Either one Eu^{2+} luminescent center or two Eu^{2+} centers have been reported.[27,29] Since only one crystallographic site is available (Ba^{2+} site), those two centers have been related to Eu^{2+} ions near a defect and to Eu^{2+} ions free of defects, respectively. Similar results have been recently published for Nd^{3+}:BMF and Nd^{3+} and Na^+ codoped BMF. The existence of two Nd^{3+} centers has been reported. They have also been associated with Nd^{3+} at a regular Ba^{2+} site and Nd^{3+} at a Ba^{2+} site distorted by the presence of a nearby charge compensator defect.[15] In the present case of Yb^{3+} ions, four clearly different non-equivalent centers have been detected by means of LT optical spectroscopy. In this respect, it should be noticed that the crystal structure of BMF shows four different Ba^{2+}-Mg^{2+} distances[11] which could eventually constitute different directions along which non local charge compensators could distort the Yb^{3+} environment. Since Yb^{3+} ions can replace for Ba^{2+} cations in the BMF crystal without causing lattice distortion (its ionic radius in octahedral coordination is notably smaller than that of Ba^{2+} ion), it can be tentatively proposed that the four Yb^{3+} centers could be attributed to different local environments in connection with the aforementioned different Ba^{2+}-Mg^{2+} distances together with the presence of charge compensators. It should also be noticed that at least for the Yb_{II} and Yb_{IV} centers, the charge compensation mechanism could not be local, while the Yb_I could correspond to a perturbed center by intrinsic charge compensators such as cation vacancies. Additional experiments are needed to establish a definitive model for the multicenter Yb^{3+} structure in BMF.

Finally, the LT fluorescence decay time of the $^2F_{5/2}$ state has been also obtained under selective excitation for the three major centers: Yb_I (in the Yb^{3+} singly doped BMF crystal) and Yb_{II} and Yb_{IV} (in both Yb^{3+} singly doped BMF and Yb^{3+}-Na^+ codoped crystal). The results are shown in Fig. 11. For the three Yb_I, Yb_{II}, and Yb_{IV} centers, single exponential decays are obtained, being their corresponding lifetimes 2.2 ms, 2.0 ms, and 2.8 ms, respectively. As seen,

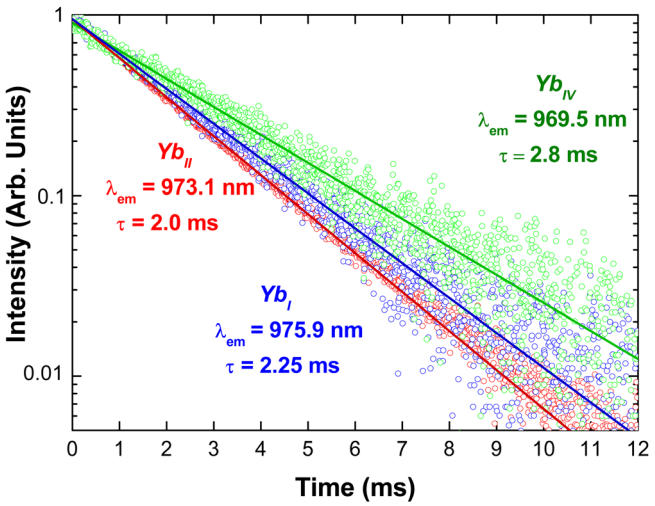

FIG. 11. (Color online) LT fluorescence decay time of the $^2F_{5/2}$ state for Yb_I, Yb_{II}, and Yb_{IV} in $BaMgF_4$. Single exponential fits are also shown.

although a clear difference is observed among the different centers, they all show comparable values as expected for centers at similar environments of the same lattice site. Considering, on the one hand, that multiphonon relaxation processes are negligible at LT and, on the other hand, that the extremely low Yb^{3+} concentration prevents radiation trapping, the aforementioned lifetime values can be considered as good approximations of the intrinsic radiative lifetimes of the $^2F_{5/2}$ state for the different Yb^{3+} centers. The obtained values are in very good agreement with those reported for Yb^{3+} in different fluoride single crystals,[30] in particular with that of $YLiF_4$.[31] At room temperature, the fluorescence decay times of the Yb_{II} and Yb_{IV} centers were also measured and fitted to single exponential decays (1.7 and 2.6 ms, respectively). Hence, the luminescence quantum efficiency for these two centers is estimated to be 0.88 and 0.93, respectively. This indicates a reduced presence of nonradiative channels from the $^2F_{5/2}$ state as corresponds to a fluoride crystal with low energy of the effective phonons.

IV. CONCLUSIONS

The incorporation of optically active Yb^{3+} ions into the nonlinear BMF fluoride crystal is established. By means of LT and site selective spectroscopy, it has been revealed that Yb^{3+} incorporates into the matrix at four nonequivalent spectroscopic centers which are tentatively related to the Ba^{2+} site, which can be affected by different, local and non local, charge compensation mechanisms. The vibronic structure related to Yb^{3+} ions has been analyzed and the energy Stark levels of the $^2F_{5/2}$ and $^2F_{7/2}$ states have been identified. The possibility to modulate the multicenter structure is demonstrated by means of codoping with Na^+, which has the effect of "cleaning" annihilating some of the dominant Yb^{3+} centers in the crystal. Since the presence of different Yb^{3+} centers can play an important role in the optical properties of the system, the present work constitutes a necessary step in the development and future optimization of Yb^{3+} doped BMF single crystals for self frequency-converter lasers.

ACKNOWLEDGMENTS

This work has been supported by Spanish MICINN under Contract Nos. MAT2010-17443 and MAT2009-06580, Comunidad de Madrid under Grant No. PHAMA-S2009/MAT-1756 and Universidad Autónoma de Madrid under Contract No. CCG10-UAM/MAT-5290. M.O Ramirez acknowledges Ramon y Cajal Contract from MICINN.

[1]T. Ellenbogen, A. Ganany-Padowicz, and A. Arie, Opt. Express **16**, 3077 (2008).
[2]D. M. Gookin, Opt. Lett. **12**(3), 196 (1987).
[3]P. Molina, M. O. Ramírez, and L. E. Bausá, Adv. Funct. Mater. **18**, 709 (2008).
[4]P. Molina, S. Alvarez-Garcia, M. O. Ramirez, J. García Solé, L. E. Bausá, H. J. Zhang, W. L. Gao, J. Y. Wang, and M. H. Jiang, Appl. Phys. Lett. **94**, 071111 (2009).
[5]A. Cordova Plaza, M. J. F. Digonnet, and H. J. Shaw, IEEE J. Quantum Electron. **23**, 262 (1987).
[6]J. J. Romero, D. Jaque, L. E. Bausá, A. A. Kaminskii, and J. García Solé, J. Lumin. **87–89**, 877 (2000).
[7]A. A. Kaminskii, D. Jaque, S. N. Bagaev, K. Ueda, J. García Solé, and J. Capmany, Quantum Electron. **29**, 95 (1999).
[8]M. O. Ramírez, P. Molina, and L. E. Bausá Opt. Mater. (in press).
[9]E. G. Villora, K. Shimamura, F. L. Jing, A. Medvedev, S. Takekawa, and K. Kitamura, Appl. Phys. Lett. **90**, 192909 (2007).
[10]K. Shimamura, E. G. Villora, H. R. Zeng, M. Nakamura, S. Takekawa, and K. Kitamura, Appl. Phys. Lett. **89**, 232911 (2006).
[11]F. Gingl, Z. Anorg. Allg. Chem. **623**, 705 (1997).
[12]K. Shimamura, E. G. Villora, K. Muramatsu, and N. Ichinose, J. Cryst. Growth. **275**(1–2), 128 (2005).
[13]S. C. Buchter, T. Y. Fan, V. Liberman, J. J. Zayhowski, M. Rothschild, E. J. Mason, A. Cassanho, H. P. Jenssen, and J. H. Burnett, Opt. Lett. **26**, 1693 (2001).
[14]E. G. Villora, K. Shimamura, K. Sumiya, and H. Ishibashi, Opt. Express **17**, 12362 (2009).
[15]E. G. Villora, P. Molina, S. Alvarez, J. V. Garcia-Santizo, M. O. Ramírez, K. Shimamura, and L. E. Bausá, J. Appl. Phys. **107**, 033106 (2010).
[16]M. Yamaga, K. Hattori, N. Kodama, N. Ishizawa, M. Honda, K. Shimamura, and T. Fukuda, J. Phys.: Condens. Matter. **13**, 10811 (2001).
[17]S. Kuck, I. Sokolska, M. Henke, T. Scheffler, and E. Osiac, Phys. Rev. B **71**, 165112 (2005).
[18]U. Brauch, A. Giesen, M. Karszewski, C. Stewen, and A. Voss, Opt. Lett. **20**, 713 (1995).
[19]A. Brenier and G. Boulon, Europhys. Lett. **55**, 647 (2001).
[20]E. Banks, A. M. Srivastava, and A. Halperin, J. Solid State. Chem. **67**, 104 (1987).
[21]V. Petit, P. Camy, J. L. Doualan, X. Portier, and R. Moncorge, Phys. Rev. B **78**, 085131 (2008).
[22]A. Lupei, V. Lupei, C. Presura, V. N. Enaki, and A. Petraru, J. Phys.: Condens. Matter **11**, 3769 (1999).
[23]E. Montoya, F. Agullo-Rueda, S. Manotas, J. Garcia Solé, and L. E. Bausá, J. Lumin. **94**, 701 (2001).
[24]M. Quilichini, Phys. Status Solidi B **68**, K155 (1975).
[25]N. Kodama, T. Hoshino, M. Yamaga, N. Ishizawa, K. Shimamura, and T. Fukuda, J. Cryst. Growth **229**, 492 (2001).
[26]F. Auzel, Opt. Mater. **19**, 89 (2002).
[27]A. Kaminskii, *Laser Crystals*, Springer Series in Optical Sciences Vol. 14 (Springer-Verlag, Berlin, 1981).
[28]M. Yamaga, T. Imai, and N. Kodama, J. Lumin. **87–89**, 992 (2000).
[29]J. M. Rey, H. Bill, D. Lovy, and H. Hagemann, J. Alloys Compd. **268**, 60 (1998).
[30]A. Bensalah, M. Ito, Y. Guyot, C. Goutaudier, A. Jouini, A. Brenier, H. Sato, T. Fukuda, and G. Boulon, J. Lumin. **122**, 444 (2007).
[31]N. Uehara, K. Ueda, and Y. Kubota, Jpn. J. Appl. Phys. **35**, 499 (1996).